IEEE Access
Multidisciplinary | Rapid Review | Open Access Journal

Received January 27, 2020, accepted February 19, 2020, date of publication March 2, 2020, date of current version March 11, 2020.

Digital Object Identifier 10.1109/ACCESS.2020.2977451

An Improved Sampling-Based Approach for Spacecraft Proximity Operation Path Planning in Near-Circular Orbit

NING CHEN, YASHENG ZHANG, ZHI LI, WENHUA CHENG, JILIAN LI, HUAFEI DIAO, WEILIN WANG, AND YUQIANG FANG

Space Engineering University, Beijing 101416, China

Corresponding author: Wenhua Cheng (cwhcn@foxmail.com)

The work of Yasheng Zhang was supported by the National Natural Science Foundation of China under Grant 61304228. The work of Yuqiang Fang was supported by the National Natural Science Foundation of China under Grant 61906213.

ABSTRACT This paper proposes an improved sampling-based approach for spacecraft proximity operation path planning under Clohessy-Wiltshire-Hill dynamics. The proposed approach is based on a modified version of the FMT* (Fast Marching Tree) algorithm with safety strategy which is divided into three parts: (1) incorporating relative ellipse to simplify the sampling state space and avoid collision with target; (2) combining internal/external ellipse-based collision detection algorithms for hovering obstacle and non-coplanar ellipse obstacle; (3) using rotating hyperplane method to handle the coplanar ellipse obstacle and uncertainty obstacle. By referring the safety strategy to simplify the state space before FMT* algorithm, the approach can reduce the complexity of path planning, especially the resampling and collision avoidance detection cyclic process in FMT*, thereby improve the planning efficiency. Two simulated scenarios, a coplanar path planning with/without coplanar ellipse obstacle, are developed to illustrate the approach. As a result, the proposed approach appears to be potential for spacecraft proximity real-time path planning as well as other complex space mission path planning generalized to different dynamics and environments, such as On-Orbit Service, and enabling a real-time computation of low-cost trajectory.

INDEX TERMS Spacecraft proximity operation, path planning, sampling-based approach, FMT*.

I. INTRODUCTION

Since 1957, humanity has entered the Space-Age, with the development of space exploration technology and space commercial activities, the number of objects in space is sharp increasing, which will make a great threat to the safety of existing satellite and the next generation space missions. According to [1], as of January 2019, there are 19,404 large objects and millions of debris in earth's orbit, and space resources and environment are facing enormous challenges. Kessler Syndrome [2] is rapidly becoming a reality. Space Debris Removal (SDR) is an effective means to keep space environment stable. The research of National Aeronautics and Space Administration (NASA) [3] shows that the Low Earth Orbit (LEO) environment can be stable with only 5-10 large debris removed from orbit each year, and SDR should focus on those targets with high mass, collision probability and orbital altitude. European Space Agency (ESA) also makes the same conclusion [4]. No matter what form of SDR, the chaser needs to operate in the proximity of target. And path planning, which refers to generating a motion sequence to guide chaser from initial state to goal state safely, is one of the key technologies in space proximity operation. Roughly, path planning can be divided into two categories: complete planning and sampling-based planning. Due to the complexity of characterizing obstacles and constraints in state space, complete planning is usually limited to handle low-dimensional problem with simple-shaped obstacles. Sampling-based planning does not need to express obstacles and constraints explicitly, but instead combines search-based sampling and performs safety verification through a collision detection algorithm. With separating the planning problem from the actual physical and geometric problems, sampling-based planning greatly accelerates the

The associate editor coordinating the review of this manuscript and approving it for publication was Rosario Pecora.

speed of planning, especially in high-dimensional problem with complex-shaped obstacles. In addition, considering the uncertainty in spacecraft proximity operation [5], chaser needs to have near real-time planning ability in order to handle various uncertainties quickly and safely. Now, the solution for handling uncertainty is mainly to use probabilistic analysis methods. Sampling-based path planning also achieves an optimal solution under probability analysis through the reduction of constraints and backward detection and evaluation, which can not only ensure the calculation efficiency, but also deal with various constraints well.

Although sampling-based path planning has not been applied in space missions, its effects and advantages for solving problems with high dynamics and uncertain environments have been verified in ground practical systems. In the Urban Challenge held by Defense Advanced Research Projects Agency (DARPA), almost all of the winners have adopted sampling-based path planning [6]–[8]. These planners have shown strong robustness and ability to deal with uncertainty constraints, indicating that sampling-based path planning is very effective for handling high-dimensional problems with strong constraints. Since the framework of path planning is universal, it seems that those research results can be applied to spacecraft path planning in theory. But the spacecraft motion is very different from ground robots, so these planners cannot be directly applied to space missions without modification. Some scholars have studied the feasibility of sampling-based path planning in space missions [9]–[12], especially the studies by Starek *et al.* [13]–[16], in which the real-time implement-ability, safety, and propellant-efficient of path planning by using FMT* or Bi-FMT* and the techniques used to adapt these algorithms to dynamically-constrained spacecraft proximity operations have been discussed in detail and thoroughly. Although these works have solved several constrained, optimal proximity operation problems under Clohessy-Wiltshire-Hill (CWH) dynamics, few have considered about what the obstacle types is in spacecraft proximity operation, and how to avoid those obstacles in path planning. The objective of this paper is to design an approach for spacecraft proximity operation with considering the obstacle type and its avoidance. In this paper, Section II introduces the system dynamics model; Then, the obstacle types are described based on the model; And, the safety strategy in path planning is proposed in detail in Sec. II. C. Section III synthesizes the safety strategy into FMT* algorithm. Finally, the proposed approach is illustrated by using two numerical experiments in Sec. IV.

II. PROBLEM FORMULATION

A. SYSTEM DYNAMICS

The spacecraft relative motion is generally described in the target orbital coordinate system (also known as Hill system which we shall henceforth refer to for brevity, see Fig.1). The Z direction (*R-bar*) is aligned with the negative of the target spacecraft inertial position vector, the Y direction (*H-bar*) is normal to the target spacecraft's orbit plane, parallel to the orbital angular momentum vector, and the X direction (*V-bar*) is the resultant vector of the cross product of Y and Z. Thus, X points in the general direction of the target spacecraft's forward orbital motion. The X vector is perfectly aligned with the velocity vector if the orbit is perfectly circular.

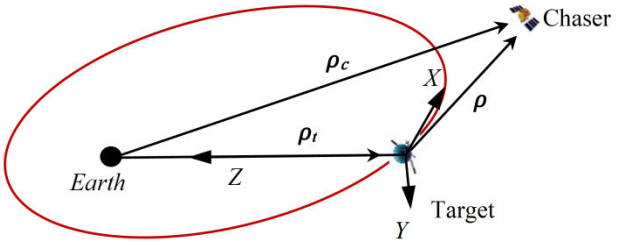

FIGURE 1. Schematic of spacecraft relative motion in Hill system.

Define $\boldsymbol{\rho} = [xyz]^T$ as the chaser position in Hill system. The relative motion equations can be illustrated as in [17].

$$\begin{aligned} \ddot{x} - 2\dot{\theta}_t\dot{z} - \dot{\theta}_t^2 x - \ddot{\theta}_t z &= -\frac{\mu}{\rho_c^3}x + (a_{cx} - a_{tx}) \\ \ddot{y} &= -\frac{\mu}{\rho_c^3}y + \left(a_{cy} - a_{ty}\right) \\ \ddot{z} + 2\dot{\theta}_t\dot{x} - \dot{\theta}_t^2 z + \ddot{\theta}_t x &= -\frac{\mu}{\rho_t^3}\rho_t - \frac{\mu}{\rho_c^3}(z - \rho_t) + (a_{cz} - a_{tz}) \end{aligned} \tag{1}$$

where ρ_c and ρ_t are the distance from earth center to chaser and target respectively; $\boldsymbol{a_c} = [a_{cx}\ a_{cy}\ a_{cz}]^T$ and $\boldsymbol{a_t} = [a_{tx}\ a_{ty}\ a_{tz}]^T$ are the acceleration of chaser and target by applied forces expressed in Hill system, respectively; μ is the geocentric gravitational constant; θ_c and θ_t are the true anomaly of chaser and target, respectively. Assuming that the target is moving on a circular or near-circular orbit without control, and the relative range between chaser and target is far less than orbital radius of target, the system dynamics equations can be described as

$$\begin{aligned} \ddot{x} - 2\omega_o\dot{z} &= a_{cx} \\ \ddot{y} + \omega_o^2 y &= a_{cy} \\ \ddot{z} + 2\omega_o\dot{x} - 3\omega_o^2 z &= a_{cz} \end{aligned} \tag{2}$$

where ω_o is the orbital angular velocity of target. Eq.(2) is the CWH model which is often used in proximity motion dynamics. Define the state $\boldsymbol{X} = [\,x\ y\ z\ \dot{x}\ \dot{y}\ \dot{z}\,]^T$ as the relative position and velocity of chaser in Hill system, the CWH equations can be described by the linear time invariant system as in [18].

$$\dot{\boldsymbol{X}} = f\,(\boldsymbol{X}, \boldsymbol{a}, t) = \boldsymbol{A}\boldsymbol{X} + \boldsymbol{B}\boldsymbol{a} \tag{3}$$

where

$$\boldsymbol{A} = \begin{bmatrix} 0 & 0 & 0 & 1 & 0 & 0 \\ 0 & 0 & 0 & 0 & 1 & 0 \\ 0 & 0 & 0 & 0 & 0 & 1 \\ 0 & 0 & 0 & 0 & 0 & 2\omega_o \\ 0 & -\omega_o^2 & 0 & 0 & 0 & 0 \\ 0 & 0 & 3\omega_o^2 & -2\omega_o & 0 & 0 \end{bmatrix}, \boldsymbol{B} = \begin{bmatrix} 0 & 0 & 0 \\ 0 & 0 & 0 \\ 0 & 0 & 0 \\ 1 & 0 & 0 \\ 0 & 1 & 0 \\ 0 & 0 & 1 \end{bmatrix}$$

It can be seen from the Eq.(2) that the y is independent of x and z, which means that the coplanar motion is decoupled from non-coplanar motion. When $\boldsymbol{a} = \mathbf{0}$, the CWH equations can be solved as

$$\begin{aligned} x &= \left(\frac{4\dot{x}_0}{\omega_o} - 6z_0\right)\sin(\omega_o t) - \frac{2\dot{z}_0}{\omega_o}\cos(\omega_o t) \\ &\quad - (3\dot{x}_0 - 6\omega_o z_0)\, t + \left(x_0 + \frac{2\dot{z}_0}{\omega_o}\right) \\ y &= \frac{\dot{y}_0}{\omega_o}\sin(\omega_o t) + y_0\cos(\omega_o t) \\ z &= -\left(3z_0 - \frac{2\dot{x}_0}{\omega_o}\right)\cos(\omega_o t) + \frac{\dot{z}_0}{\omega_o}\sin(\omega_o t) + \left(4z_0 - \frac{2\dot{x}_0}{\omega_o}\right) \end{aligned} \tag{4}$$

where $[\, x_0 \;\; y_0 \;\; z_0 \;\; \dot{x}_0 \;\; \dot{y}_0 \;\; \dot{z}_0 \,]^T$ is the initial state of chaser in Hill system. Thus, the coplanar motion can be described as in [19].

$$\frac{(x - X_0)^2}{(2S)^2} + \frac{(z - Z_0)^2}{S^2} = 1 \tag{5}$$

where

$$X_0 = x_0 + \frac{2\dot{z}_0}{\omega_o} - (3\dot{x}_0 - 6\omega_o z_0)\, t \quad Z_0 = 4z_0 - \frac{2\dot{x}_0}{\omega_o}$$

$$S = \sqrt{\left(3z_0 - \frac{2\dot{x}_0}{\omega_o}\right)^2 + \left(\frac{\dot{z}_0}{\omega_o}\right)^2}$$

Eq.(5) shows that the coplanar motion of chaser in Hill system is an ellipse determined by X_0, Z_0 and S. The center of ellipse is (X_0, Z_0), which moves parallel to the *V-bar* over time. The semi-major axis of ellipse is $2S$ and twice the semi-minor axis. In particular, when

$$\dot{x}_0 = 2\omega_o z_0 \tag{6}$$

The coplanar motion equation becomes

$$\frac{\left(x - x_0 - \frac{2\dot{z}_0}{\omega_o}\right)^2}{4\,(z_0)^2 + 4\left(\frac{\dot{z}_0}{\omega_o}\right)^2} + \frac{z^2}{(z_0)^2 + \left(\frac{\dot{z}_0}{\omega_o}\right)^2} = 1 \tag{7}$$

And the center of ellipse is fixed in one point of *V-bar*, see Fig.2.

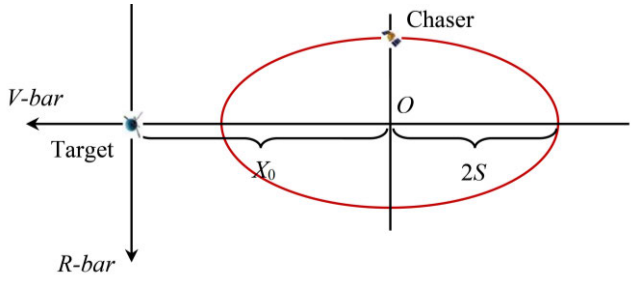

FIGURE 2. Schematic of relative ellipse in Hill system.

In addition, different X_0 and S determine the specific shape of ellipse and the minimum distance between chaser and target (see Appendix A for calculation).

B. OBSTACLE TYPES

Considering the system dynamics described above, the obstacles in spacecraft proximity path planning can be divided into four types roughly: hovering obstacle ($S = 0$), non-coplanar ellipse obstacle ($y \neq 0$), coplanar ellipse obstacle ($y = 0$), and uncertainty obstacle, as shown in Fig.3

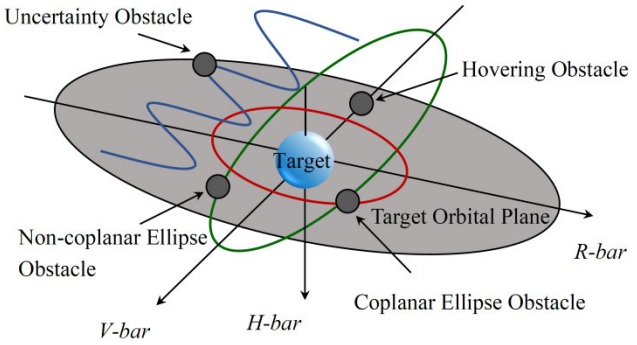

FIGURE 3. Four obstacle types in spacecraft autonomous proximity path planning.

Hovering obstacle refers to an obstacle that is invariant to target, and appears as a fixed area in Hill system. Coplanar ellipse obstacle refers to those moving on *V-R-bar* plane, and its configuration relative to target is a closed ellipse. The configuration of non-coplanar ellipse obstacle is also a closed ellipse, but it locates on a certain inclined plane relative to the *V-R-bar* plane, as a three-dimensional ellipse. Uncertainty obstacle is an obstacle that cannot be maintained for a stable configuration relative to target. And, if the designed trajectory is not intersecting with those configurations, then the spacecraft must be safe in proximity operation.

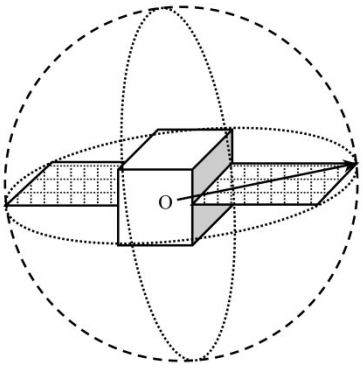

FIGURE 4. Schematic of spacecraft envelope.

C. SAFETY STRATEGY

In order to better make safety strategy, define envelope as a sphere which completely encloses the spacecraft (see Fig.4). In this paper, we think of collision as the intersection of two envelopes. In addition, the chaser is considered as a point, and the radius of target or obstacle envelope becomes twice the original. Thus, it is possible to ensure that the chaser would

not collide with target or obstacle even if the planned trajectory is tangent to the envelope. In this section, we propose a safety strategy which consists of three parts to guarantee path planning solution safety.

1) COLLISION AVOIDANCE FOR TARGET BASED ON RELATIVE ELLIPSE

Relative position configuration between chaser and target under different initial conditions has been analyzed in detail above. It can be found that when the relative state of chaser and target meets certain conditions (see Eq.(6)), the chaser will form a stable ellipse configuration with respect to target. And, by setting the minimum distance constraint, it can be ensuring that the chaser does not collide with target when moving along the ellipse.

Based on this, the state space is simplified as a set of states that satisfies Eq.(6). In this way, in path planning, it is no longer necessary to consider the collision between chaser and target, but only the conflict with obstacles. This measure can simplify the cyclic process by referring the safety analysis to initial conditions of path planning, and improve the efficiency. Fig.5 shows the collision avoidance for target based on relative ellipse.

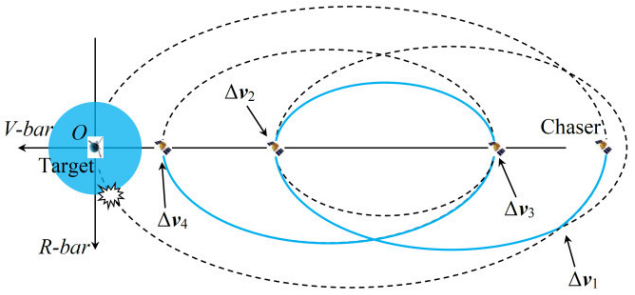

FIGURE 5. Collision avoidance for target based on relative ellipse.

2) INTERNAL/EXTERNAL ELLIPSE-BASED COLLISION DETECTION

In this section, we give a measure to deal with the collision detection problem and determining whether the relative ellipse above intersects with the hovering obstacle or non-coplanar ellipse obstacle. Traditionally, the collision detection is equivalent to judging whether an ellipse and a circle intersect or not, and necessary to solve a system of binary quadratic equations, which is relatively complicated and affects the calculation efficiency. To this end, we propose an internal/external ellipse-based collision detection algorithm, as shown in Fig.6 (taking coplanar path planning as example).

In Eq.(7), it is easy to find that the ratio of semi-major axis and semi-minor axis is 2. Assuming the obstacle envelope radius is R, and define internal/external ellipse as follows (see Fig.6).

Definition 1 (internal ellipse): The internal ellipse is to reduce the semi-major axis and semi-minor axis length of relative ellipse by $2R$ and R respectively, and keep the ratio to the same. The internal ellipse equation is

$$\frac{(x - X_0)^2}{(2S - 2R)^2} + \frac{z^2}{(S - R)^2} = 1 \tag{8}$$

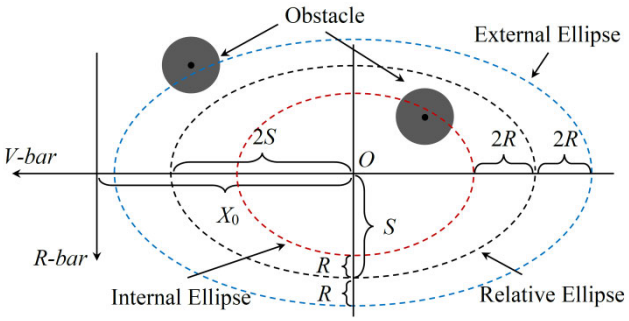

FIGURE 6. Internal/external ellipse-based collision detection.

Definition 2 (external ellipse): The external ellipse is to increase the semi-major axis and semi-minor axis length of relative ellipse by $2R$ and R respectively, and keep the ratio to the same. Its equation is

$$\frac{(x - X_0)^2}{(2S + 2R)^2} + \frac{z^2}{(S + R)^2} = 1 \tag{9}$$

It is easy to obtain that when the center of obstacle envelope is located within the internal ellipse, the relative ellipse will certainly not intersect with obstacle; similarly, when the center of obstacle envelope is outside the external ellipse, the relative ellipse does not also intersect with obstacle. Thus, the condition that relative ellipse does not intersect with obstacle can be expressed as

$$\begin{aligned} &\frac{(x_{obs} - X_0)^2}{(2S - 2R)^2} + \frac{z_{obs}^2}{(S - R)^2} < 1 \\ &or \ \frac{(x_{obs} - X_0)^2}{(2S + 2R)^2} + \frac{z_{obs}^2}{(S + R)^2} > 1 \end{aligned} \tag{10}$$

where (x_{obs}, z_{obs}) is the center location of obstacle envelope.

In this way, the solution of solving binary quadratic equation is transformed into the judgment of relationship between the obstacle center and the internal/external ellipse, which can greatly simplify the calculation process. When extended to non-coplanar conditions, collision detection can also be carried out using the internal/external ellipse method. As shown in Fig.7, the obstacles are projected on three planes and analyzed separately.

Define H as the radius of relative ellipse projection on *R-H-bar* plane, we can know from the Eq.(4) that

$$H = \sqrt{y^2 + \left(\frac{\dot{y}}{\omega_o}\right)^2} \tag{11}$$

And the angle between relative ellipse and *V-R-bar* plane can be described as

$$\alpha = \arctan \frac{H}{2S} \tag{12}$$

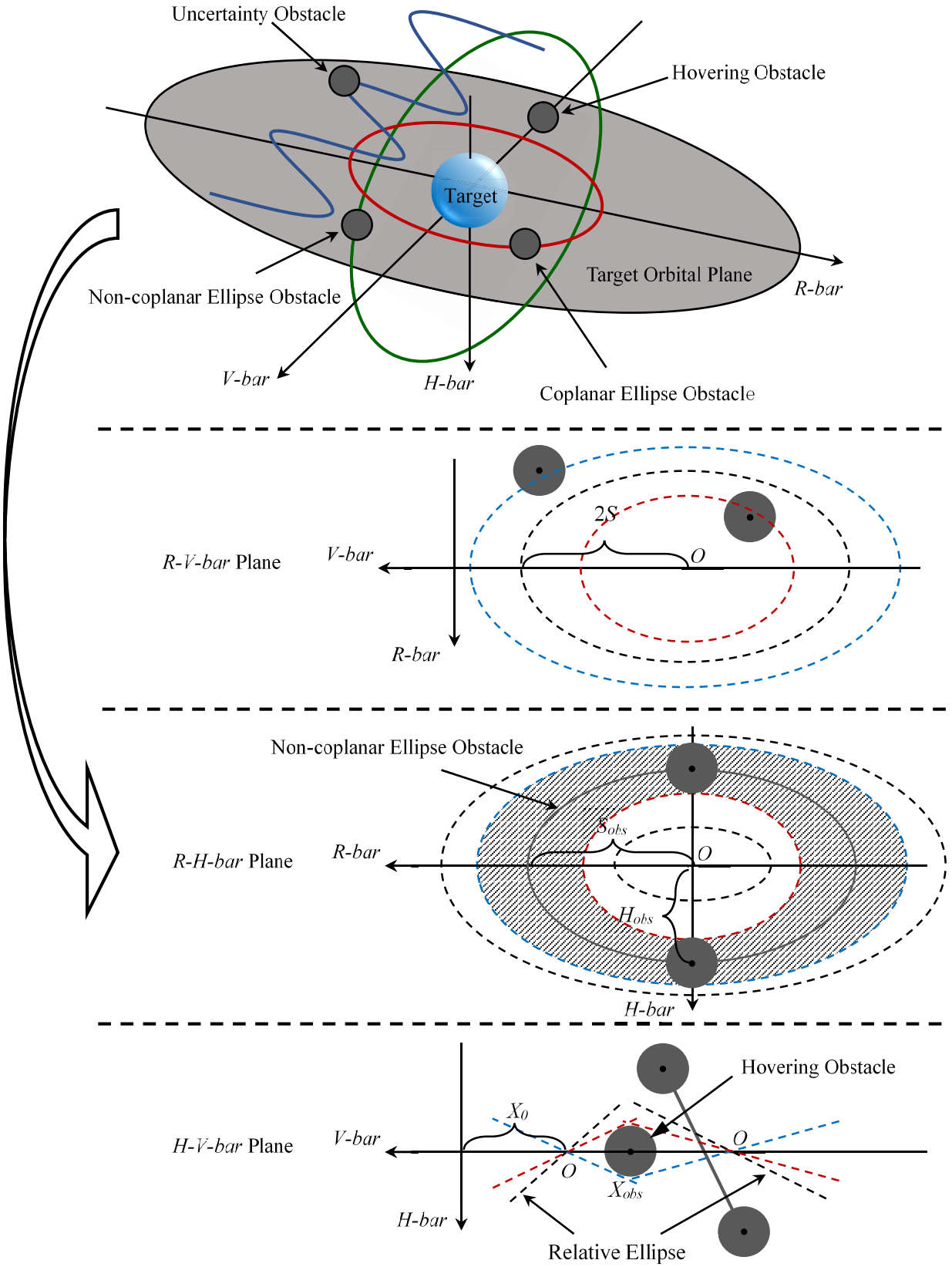

FIGURE 7. Non-coplanar ellipse obstacle collision detection.

Define the projection of non-coplanar ellipse obstacle on *R-H-bar* plane be

$$\frac{y^2}{H_{obs}^2}+\frac{z^2}{S_{obs}^2}=1 \tag{13}$$

Therefore, the internal/external ellipse in *R-H-bar* plane can be described as

$$\begin{aligned}
&\text{Internal Ellipse}\begin{cases}\dfrac{y^2}{(H_{obs}-R)^2}+\dfrac{z^2}{\left(S_{obs}-\dfrac{S_{obs}}{H_{obs}}R\right)^2}=1 \\ (H_{obs}<S_{obs}) \\ \dfrac{y^2}{\left(H_{obs}-\dfrac{H_{obs}}{S_{obs}}R\right)^2}+\dfrac{z^2}{(S_{obs}-R)^2}=1 \\ (H_{obs}>S_{obs})\end{cases} \\
&\text{External Ellipse}\begin{cases}\dfrac{y^2}{(H_{obs}+R)^2}+\dfrac{z^2}{\left(S_{obs}+\dfrac{S_{obs}}{H_{obs}}R\right)^2}=1 \\ (H_{obs}<S_{obs}) \\ \dfrac{y^2}{\left(H_{obs}+\dfrac{H_{obs}}{S_{obs}}R\right)^2}+\dfrac{z^2}{(S_{obs}+R)^2}=1 \\ (H_{obs}>S_{obs})\end{cases}
\end{aligned} \tag{14}$$

Thus, it can be obtained that the sufficient condition which making the chaser does not intersect with non-coplanar ellipse obstacle is

$$\begin{aligned}
&\begin{cases}H<\min\left(H_{obs}-\dfrac{H_{obs}}{S_{obs}}R\ H_{obs}-R\right) \\ S<\min\left(S_{obs}-\dfrac{S_{obs}}{H_{obs}}R\ S_{obs}-R\right)\end{cases} \\
or\ &\begin{cases}H>\max\left(H_{obs}+\dfrac{H_{obs}}{S_{obs}}R\ H_{obs}+R\right) \\ S>\max\left(S_{obs}+\dfrac{S_{obs}}{H_{obs}}R\ S_{obs}+R\right)\end{cases}
\end{aligned} \tag{15}$$

In addition, it can also be seen from Fig.7 that in order to avoid intersection between relative ellipse trajectory and hovering obstacle, the distance between relative ellipse center and hovering obstacle center, as well as the angle between relative ellipse and *V-R-bar* plane, needs to meet some certain conditions.

Define X_{obs} as the center position of hovering obstacle in *V-bar*, then the critical angle is

$$\alpha_{\min}=\arcsin\frac{R}{|X_0-X_{obs}|} \tag{16}$$

Thus, the sufficient condition that the chaser does not intersect with hovering obstacle can be given as

$$\begin{cases}\alpha>\alpha_{\min} \\ |X_{obs}-X_0|<2S+R\end{cases} \quad or\ |X_{obs}-X_0|>2S+R \tag{17}$$

3) COPLANAR ELLIPSE AND UNCERTAINTY OBSTACLE AVOIDANCE STRATEGY

Since the spacecraft, also including debris, becoming smaller and smaller, it is difficult to determine their orbit with ground-based or space-based observations, leading to a greatly increased probability of uncertainty obstacle in spacecraft proximity operation. In addition, as we all known, the cost of non-coplanar orbit maneuver is much higher than coplanar orbit maneuver. Thus, we consider the coplanar path planning result as the standard trajectory, and make the chaser moving along the trajectory as much as possible. In order to achieve those goal, the rotating hyperplane method [20] is used to avoid such coplanar ellipse and uncertainty obstacles during chaser's proximity operation to target, as shown in Fig.8.

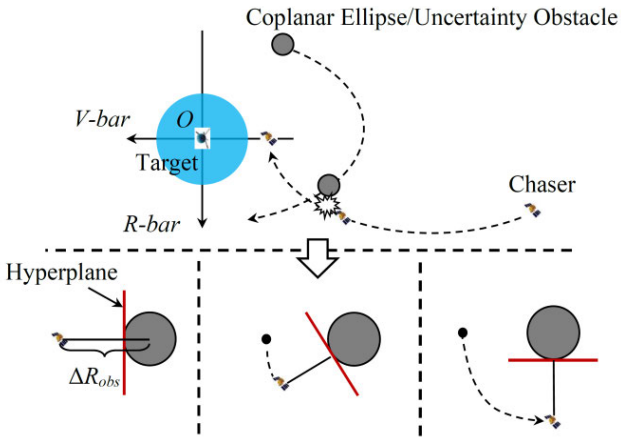

FIGURE 8. Coplanar ellipse and uncertainty obstacle avoidance based rotating hyperplane method.

When the chaser moves into a certain region of obstacle, its state is changed to ensure the distance to target is always larger than the safety threshold ΔR_{obs}. After bypassing or starting to move away from obstacle, the chaser is returned to the standard trajectory.

Define $\boldsymbol{\rho}_{obs}$ as the center position of obstacle. And, the rotating hyperplane method can be expressed as: When the distance between chaser and target meets

$$\left|\boldsymbol{\rho}-\boldsymbol{\rho}_{obs}\right|\le\Delta R_{obs} \tag{18}$$

Then, the chaser's state is changed by the control system to satisfy

$$\frac{\left(\dot{\boldsymbol{\rho}}-\dot{\boldsymbol{\rho}}_{obs}\right)\cdot\left(\boldsymbol{\rho}-\boldsymbol{\rho}_{obs}\right)}{\left|\dot{\boldsymbol{\rho}}-\dot{\boldsymbol{\rho}}_{obs}\right|\cdot\left|\boldsymbol{\rho}-\boldsymbol{\rho}_{obs}\right|}\le 0 \tag{19}$$

III. PLANNING ALGORITHM

In this section, we propose a modified version of the FMT* algorithm which incorporates our safety strategy.

A. BASIC DESCRIPTION

Define the state space $\boldsymbol{X}$ as chaser's position and velocity in Hill system, and $\boldsymbol{X}_{obstacle}$ is the set of states which will make chaser result in a collision with target or obstacle. $\boldsymbol{X}_{free}$ is the complement of $\boldsymbol{X}_{obstacle}$ in $\boldsymbol{X}$, and the set of states for

sampling. $\boldsymbol{X}_{initial}$ is the initial state of chaser, and $\boldsymbol{X}_{goal}$ is the goal of mission presented in $\boldsymbol{X}$.

Define the state path $\boldsymbol{X}(t)$ is a function over time which is determined by the acceleration of chaser as described in Sec.II.A. In this paper, we employ the Starek's work [16] as the definition of path planning problem which is formulated as follows.

Given: $\boldsymbol{X}_{initial}, t_0, \boldsymbol{X}_{goal}$, **and** $\boldsymbol{X}_{free}$

Cost function: $J\left(\boldsymbol{a}\left(t\right), t_f\right) = \sum_{i=1}^{N} \|\Delta \boldsymbol{v}_i\|$

Constraints:

$$\begin{aligned} &\boldsymbol{X}\left(t_0\right) = \boldsymbol{X}_{initial}, \boldsymbol{X}\left(t_f\right) \in \boldsymbol{X}_{goal} \\ &\forall t \in \left[\, t_0 \;\; t_f \,\right], \boldsymbol{X}\left(t\right) \in \boldsymbol{X}_{free} \\ &\dot{\boldsymbol{X}}\left(t\right) = f\left(\boldsymbol{X}\left(t\right), \boldsymbol{a}\left(t\right), t\right) = \boldsymbol{A}\boldsymbol{X} + \boldsymbol{B}\boldsymbol{a} \\ &T_{plan-\min} \le t_f \le T_{plan-\max} \\ &\forall i \in [1, 2, \cdots, N], \|\Delta \boldsymbol{v}_i\| \le \Delta v_{\max}, \\ &\sum_{i=1}^{N} \|\Delta \boldsymbol{v}_i\| \le \Delta V_{\max} \end{aligned}$$

Where $[T_{plan-\min} \;\; T_{plan-\max}]$ is the mission completion time interval; $\Delta \boldsymbol{V} = [\Delta \boldsymbol{v}_1, \Delta \boldsymbol{v}_2, \ldots, \Delta \boldsymbol{v}_N]^{\mathrm{T}}$ is the chaser's multi-pulses maneuver in proximity operation; $\Delta v_{\max}$ is the maximum single pulse of chaser and $\Delta V_{\max}$ is the maximum total pulses of chaser.

B. STATE SPACE SIMPLIFICATION

We now elaborate on the state space simplification with our work in Sec. II. As mentioned above, the state space is defined as

$$\boldsymbol{X} = \left\{\left(x \;\; y \;\; z \;\; \dot{x} \;\; \dot{y} \;\; \dot{z}\right)\right\} \tag{20}$$

Simplification 1(State Space Ellipse Processing): Considering the relative ellipse configuration, the state space is simplified as a set of states that satisfies Eq.(6), named $\boldsymbol{X}_{ellipse}$.

$$\boldsymbol{X}_{ellipse} = \left\{\left(x \;\; y \;\; z \;\; \dot{x} \;\; \dot{y} \;\; \dot{z}\right) | \dot{x} = 2\omega_o z\right\} \tag{21}$$

Simplification 2(Coplanar planning): When the chaser only performs path planning in target orbital plane, the state space can be simplified as

$$\boldsymbol{X}_{ellipse} = \left\{\left(x \;\; 0 \;\; z \;\; \dot{x} \;\; 0 \;\; \dot{z}\right) | \dot{x} = 2\omega_o z\right\} \tag{22}$$

Simplification 3(Relative Ellipse State Equivalence): Considering the closeness of relative ellipse, which means that every state point on ellipse has a same configuration or movement for target in Hill system, we can simplify the state space by converting the ellipse state into the endpoint of semi-major axis, and making all sampling point located on *V-bar* with a velocity along *R-bar*. Then, the state space is further simplified as

$$\boldsymbol{X}_{ellipse} = \left(x \;\; 0 \;\; 0 \;\; 0 \;\; 0 \;\; \dot{z}\right) \tag{23}$$

For each relative ellipse, its minimum distance to target can be calculated with Appendix A. By comparing the minimum distance and the radius of target envelope, we can eliminate those states result in collision with target, and achieve a new state space $\boldsymbol{X}_{safe}$ for sampling.

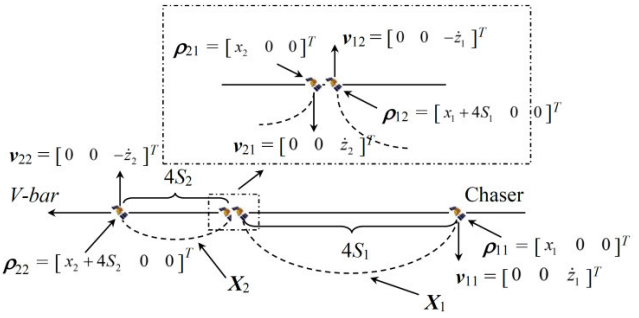

FIGURE 9. Neighborhood confirmation of simplified state.

C. NEIGHBORHOOD OF SIMPLIFIED STATE

With the simplification above, the state space is transformed as a set of points in *V-bar*, and each point has a velocity along *R-bar* (see Fig.9). Thus, the neighborhood of a state can be described as follows.

Define

$\boldsymbol{X}_1 = [x_1 \;\; 0 \;\; 0 \;\; 0 \;\; 0 \;\; \dot{z}_1]^T$

$\boldsymbol{X}_2 = [x_2 \;\; 0 \;\; 0 \;\; 0 \;\; 0 \;\; \dot{z}_2]^T$

Then, according to system dynamics in Sec. II. A, the endpoints' position and velocity of the relative ellipse major axis can be expressed as shown in Fig.9.

Where

$$S_1 = (z_1)^2 + \left(\frac{\dot{z}_1}{\omega_o}\right)^2, S_2 = (z_2)^2 + \left(\frac{\dot{z}_2}{\omega_o}\right)^2$$

Thus, in this paper, we consider that $\boldsymbol{X}_1$ and $\boldsymbol{X}_2$ are neighborhoods when their states meet the following conditions.

$$\begin{aligned} \Delta v &= \|\boldsymbol{v}_{12} - \boldsymbol{v}_{21}\| = \dot{z}_1 + \dot{z}_2 \le \Delta v_{\max} \\ \Delta \rho &= \left\|\boldsymbol{\rho}_{12} - \boldsymbol{\rho}_{21}\right\| = |x_1 + 4S_1 - x_2| \le \xi \end{aligned} \tag{24}$$

where ξ is a certain positive value.

D. MODIFIED FMT*ALGORITHM

The modified FMT* algorithm, tailored with our strategy, is presented as Algorithm 1 and Algorithm 2.

IV. NUMERICAL EXPERIMENTS

In this section, two simulated scenarios are developed to illustrate the approach proposed above.

A. SIMULATION SETUP

All relevant simulation parameters in this paper are listed as follow.

$$\begin{aligned} \boldsymbol{X}_{initial} &= \left(-100 \;\; 0 \;\; 0 \;\; 0 \;\; 0 \;\; 0\right) \\ \boldsymbol{X}_{goal} &= \left\{\left(x \;\; y \;\; z \;\; \dot{x} \;\; \dot{y} \;\; \dot{z}\right) \middle| \begin{matrix} -10 < x < -9.5 \\ \dot{x} = \dot{y} = \dot{z} = y = z = 0 \end{matrix}\right\} \\ R_{Target} &= 8m \end{aligned}$$

Algorithm 1 The Modified FMT*: Computes a Minimal-Cost Trajectory

Given initial state $X_{initial}$, goal state region X_{goal}, position threshold ξ, and maximum velocity increment Δv_{max}
State space simplification: $X \rightarrow X_{ellipse}$
Collision avoidance for target: $X_{ellipse} \rightarrow X_{safe}$
Taking samples in X_{safe} by using Halton sequence as X_S, and define S is the set of $X_{initial}$, X_{goal}, and X_S
Generate the state sets $\{S_{tree}, S_{check}, S_{cut}\}$ and S_{tree}, S_{check}, and S_{cut} are similar to the V_{open}, $V_{unvisited}$, and V_{closed} in [16]
While do
  Generate the intersection S_{meet} of S_{tree} and X_{goal}
  If S_{meet} is not empty
    For each state in S_{meet}, compute the $J_{initial}$
    Find the x_{meet} which result in minimum total cost
    Take x_{meet} as end point of the S_{tree}, and obtain tree T connecting $X_{initial}$ and X_{goal}
  If S_{meet} is empty
    Update $\{S_{tree}, S_{check}, S_{cut}\}$ with Algorithm 2
While done

Algorithm 2 Updates the State Sets $\{S_{tree}, S_{check}, S_{cut}\}$

Find the state $S_{nearest}$ in S_{tree} which result in minimum cost to $X_{initial}$
Find the neighborhood X_{near} of $S_{nearest}$ in S_{check} based on given threshold v_{max} and ξ
For each state x in X_{near}
  Find the neighborhood x_{near} of x in S_{tree}
  Find the state $x_{nearest}$ in x_{near} which result in minimum cost to x
Remove all successful state x from S_{check} and Add them to S_{tree}
Remove $S_{nearest}$ from S_{tree} and add it to S_{cut}

$$R = 5m$$
$$\xi = 0.01m$$
$$\Delta v_{\max} = 0.5m/s$$
$$\Delta V_{\max} = 50m/s$$

In order to make the simulation clear and simple, we design the following data structure to represent the feature information of sampling state points.

$$Node_i = \{\, i\ x\ y\ z\ \dot{x}\ \dot{y}\ \dot{z}\ iftoinitial\ iftogoal\ j\ J_{ij}\ J_{initial}\ J_{goal} \,\}$$

where i is number of sampling state point; $iftoinitial/iftogoal$ is the judgement mark of connection to $X_{initial}/X_{goal}$, and $iftoinitial/iftogoal = 0$ means that the sampling one is not connected with $X_{initial}/X_{goal}$, while $iftoinitial/iftogoal = 1$ means that connected; j is the number of forward connected sampling state point, and define that $j = 0$ means initial state, $j = -1$ means goal state, and $j = -2$ means no forward connection; J_{ij} is the cost between $Node_i$ and $Node_j$; $J_{initial}/J_{goal}$ is the cost to $X_{initial}/X_{goal}$.

In our paper, all simulations are implemented in MATLAB ®2015b and run on a PC with Intel(R) Core(TM) i7-4720HQ CPU operated by Windows 10, clocked at 2.60 GHz, and equipped with 8.0 GB of RAM.

B. PATH PLANNING WITHOUT COPLANAR ELLIPSE OBSTACLE

Consider the scenario that coplanar near-field approaches of a chaser spacecraft with the hovering obstacle and non-coplanar ellipse obstacle in close proximity to a target moving on a circular GEO trajectory, as shown in Fig.10.

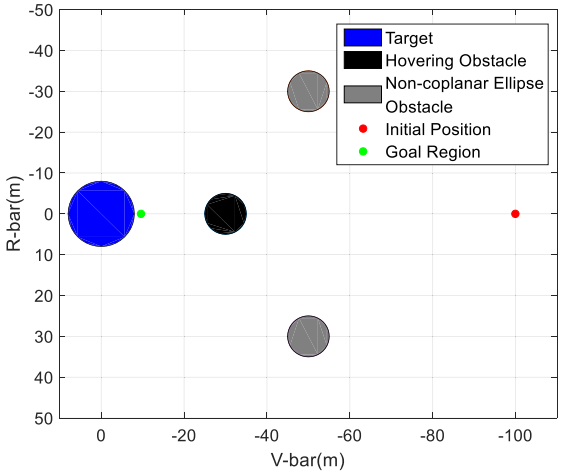

FIGURE 10. Illustration of coplanar path planning simulation scenario.

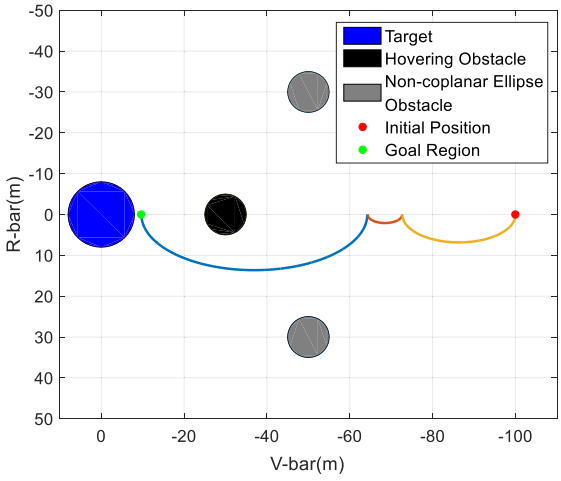

FIGURE 11. Coplanar path planning solution of the scenario using FMT* with $n = 10000$.

A representative solution to the scenario with proposed planning algorithm is shown in Table 1 and Fig.11. As shown, the planner successfully finds safe trajectories within the obstacles in scenario, and the planning time is 0.758s. The chaser approaches the goal region after four maneuvers, and the total energy consumption is 3.28e-03m/s.

TABLE 1. Coplanar path planning solution of the scenario using FMT* with n = 10000.

i	ρ (m/s)	v (m/s)	Δv (m/s)	Total Δv (m/s)
0	(-100,0,0)	(0,0,0)	4.967e-04	4.967e-04
48	(-72.656,0,0)	(0,0,1.523e-04)	6.492e-04	1.146e-03
2632	(-64.221,0,0)	(0,0,9.912e-04)	1.143e-03	2.289e-03
-1	(-9.687,0,0)	(0,0,0)	9.912e-04	3.280e-03

TABLE 2. Path planning solutions with different n.

n = 5000	n = 20000
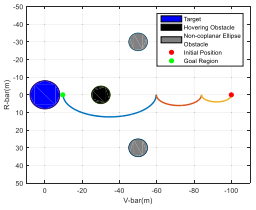	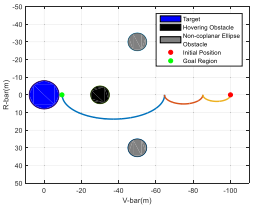
T=0.228s, Δv=3.276e-03m/s	T=4.139s, Δv=3.281e-03m/s

In order to better illustrate the algorithm effectiveness, we change the number of samples to 5000 and 20000, and the radius of the obstacle area is doubled. The simulation results are shown in Table 2 and Fig.12 separately.

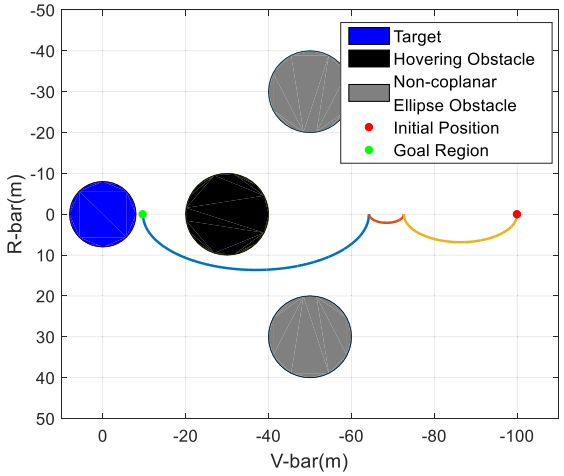

FIGURE 12. Coplanar path planning solution with doubled obstacle radius.

In Table 2, we can see that as the number of samples increases, the planning time becomes longer, which is mainly due to the ellipse consumption of sampling space and obstacle collision detection. And if those two parts have been done in offline planning, which means that the sampling state space is known, the planning time consumes 0.026s, 0.024s, and 0.022s, respectively. It can be seen that the proposed algorithm has great potential in real-time planning.

As shown in Fig.12, although the obstacle region becomes larger, the planning algorithm can still get the approach path quickly, which illustrates the effectiveness of algorithm. In addition, it can be found that the planning time becomes shorter. It is because the larger obstacle region is resulting in the reduction of effective sampling states, which in turn reduces the calculation and makes the planning time correspondingly shorter.

C. PATH PLANNING WITH COPLANAR ELLIPSE OBSTACLE

Define coplanar ellipse obstacle configuration as follow.

$$\frac{x^2}{50^2} + \frac{z^2}{25^2} = 1$$

And the rest of the simulation settings are the same as in scenario above. Since obstacle avoidance requires real-time control, the classic PD control algorithm is used in this simulation. The additional simulation parameters are listed as follow.

$$K_P = 0.002 \quad K_D = 0.004 \quad \Delta R_{obs} = 10m$$

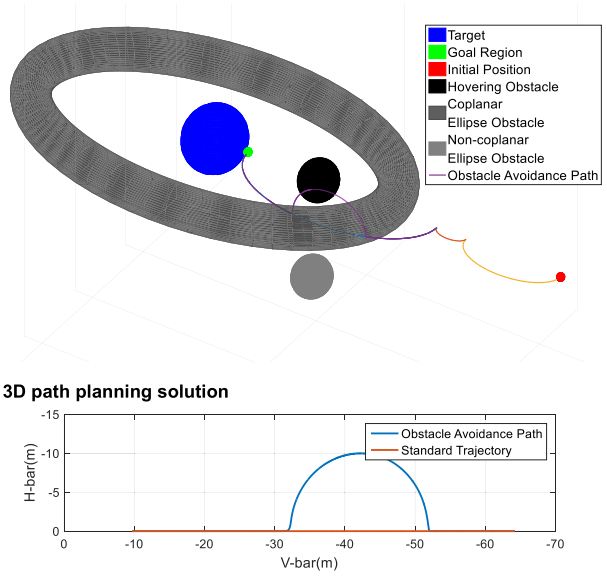

a) 3D path planning solution

b) Path planning solution in V-H-bar plane

FIGURE 13. Coplanar path planning solution with coplanar ellipse obstacle.

The simulation results of obstacle avoidance based on the rotating hyperplane are shown in Fig.13. It can be seen that during chaser moving along the standard trajectory, if the distance to obstacle is less than the threshold ΔR_{obs}, the chaser would change its trajectory and stay away from the obstacle under control system. In this process, the trajectory projection on target orbital plane is unchanged, and only the velocity in *H-bar* direction is changed. After the chaser passes obstacle, the position and velocity in *H-bar* direction is restored to 0, and the chaser continues to move along the standard trajectory.

V. CONCLUSION

An improved sampling-based approach for spacecraft proximity operation path planning under CWH dynamics is studied. The approach consists of a modified version of the FMT* algorithm with safety strategy. The proposed strategy is specific to the obstacle types which are analyzed

and listed in Sec.II.B, and can be divided into three parts: (1) collision avoidance for target based on relative ellipse in Hill system; (2) internal/external ellipse-based collision detection algorithms for hovering obstacle and non-coplanar ellipse obstacle; (3) coplanar ellipse and uncertainty obstacle avoidance by rotating hyperplane method. In our approach, before sampling the state space, we firstly use the strategy to simplify the state space, and make it as a set of states which locates on *V-bar* and does not collide with target, hovering obstacle, and non-coplanar ellipse obstacle. Then, the FMT* algorithm is applied on state space to construct a safe and propellant efficient solution trajectory that satisfied constraints from initial position to goal region.

By referring the safety strategy to simplify the state space before FMT* algorithm, our approach can reduce the complexity of path planning, especially the resampling and collision avoidance detection cyclic process in FMT*, thereby improve the planning efficiency. It appears to be potential for spacecraft proximity real-time path planning. In addition, the proposed approach is flexible enough to well deal with other path planning generalized to different dynamics and environments as long as the constraints and cost evaluation function remains efficient, and enabling a real-time computation of low-cost trajectory.

The approach proposed in this paper can be further researched in several aspects. For example, considering more constraints such as attitude constraints in which the chaser is pointing to target, solar array is pointing to sun, and antenna is pointing to ground station, etc. Also, considering the orbit perturbation, targets in ellipse orbit, higher-order dynamic model, and computer memory and performance onboard provides more interesting research areas. Those future research can expand the applicability of our approach to more general situation, and evaluate its true benefits to spacecraft path planning.

APPENDIX

Using triangular transformation, chaser's position in target orbital plane can be expressed as

$$\begin{aligned} x &= X_0 + 2S\cos\alpha \\ z &= S\sin\alpha \end{aligned} \quad \alpha \in [\,0\ 2\pi\,) \tag{A1}$$

Thus, the relative range between chaser and target is

$$\begin{aligned} \rho &= \sqrt{x^2+z^2} = \sqrt{(X_0+2S\cos\alpha)^2+(S\sin\alpha)^2} \\ &= \sqrt{X_0^2+S^2+3S^2\cos^2\alpha+4X_0S\cos\alpha} \\ &= \sqrt{S^2-\frac{1}{3}X_0^2+\frac{4}{3}\left(X_0+\frac{3}{2}S\,cos\alpha\right)^2} \\ &= \sqrt{S^2-\frac{1}{3}X_0^2+\frac{4}{3}\left|X_0+\frac{3}{2}S\cos\alpha\right|^2} \end{aligned} \tag{A2}$$

Consider

$$\cos\alpha \in [\,-1\ 1\,]$$

TABLE 3. Minimum distance between chaser and target under different initial conditions.

Initial condition	Minimum distance
$X_0 > 2S$	$X_0 - 2S$
$\frac{3}{2}S < X_0 < 2S$	$2S - X_0$
$0 < X_0 < \frac{3}{2}S$	$\sqrt{S^2 - \frac{1}{3}X_0^2}$
$X_0 = 0$	S
$-\frac{3}{2}S < X_0 < 0$	$\sqrt{S^2 - \frac{1}{3}X_0^2}$
$-2S < X_0 < -\frac{3}{2}S$	$2S + X_0$
$X_0 < -2S$	$-2S - X_0$

If

$$|X_0| \le \frac{3}{2}S$$

Then, the absolute value term under square root can be taken to 0, and minimum relative range is

$$\begin{aligned} \rho_{\min} &= \sqrt{S^2-\frac{1}{3}X_0^2+\frac{4}{3}\left|X_0+\frac{3}{2}S\cos\alpha\right|^2_{\min}} \\ &= \sqrt{S^2-\frac{1}{3}X_0^2} \end{aligned}$$

Conversely, if

$$|X_0| > \frac{3}{2}S$$

The minimum relative range becomes

$$\begin{aligned} \rho_{\min} &= \begin{cases} \sqrt{S^2-\frac{1}{3}X_0^2+\frac{4}{3}\left(X_0-\frac{3}{2}S\right)^2} & X_0 > \frac{3}{2}S \\ \sqrt{S^2-\frac{1}{3}X_0^2+\frac{4}{3}\left(X_0+\frac{3}{2}S\right)^2} & X_0 < -\frac{3}{2}S \end{cases} \\ &= \begin{cases} |X_0-2S| & X_0 > \frac{3}{2}S \\ |X_0+2S| & X_0 < -\frac{3}{2}S \end{cases} \end{aligned}$$

Relative position configuration between chaser and target under different initial conditions is shown in Table 3.

REFERENCES

[1] *Orbital Debris Quarterly News*, NASA, Washington, DC, USA, May 2019.

[2] D. J. Kessler and B. G. Cour-Palais, "Collision frequency of artificial satellites: The creation of a debris belt," *J. Geophys. Res.*, vol. 83, no. A6, pp. 2637–2646, 1978, doi: 10.1029/JA083iA06p02637.

[3] J. C. Liou, "USA space debris environment, operations, and research updates," in *Proc. 52th Session Sci. Tech. Subcommittee*. Vienna, Austria: United Nations Committee Peaceful Uses Outer Space, 2015, pp. 1–14.

[4] B. Bastida and H. Krag, "Analyzing the criteria for a stable environment," in *Proc. AAS/AIAA Astrodynamics Spec. Conf.*, Girdwood, Alaska, 2011, pp. 1–13.

[5] C. M. Jewison, "Guidance and control for multi-stage rendezvous and docking operations in the presence of uncertainty," Ph.D. dissertation, Dept. Aeronaut. Astronaut., MIT, Cambridge, MA, USA, 2017.

[6] C. Urmson, J. Anhalt, D. Bagnell, C. Baker, R. Bittner, M. N. Clark, J. Dolan, D. Duggins, T. Galatali, C. Geyer, and M. Gittleman, "Autonomous driving in urban environments: Boss and the urban challenge," *J. Field Robot.*, vol. 25, no. 8, pp. 425–466, Aug. 2008, doi: 10.1002/rob.20255.
[7] M. Montemerlo, J. Becker, and S. Bhat, "Junior: The stanford entry in the urban challenge," *J. Field Robot.*, vol. 25, no. 9, pp. 569–597, 2008, doi: 10.1007/978-3-642-03991-1_3.
[8] Y. Kuwata, S. Karaman, and J. Teo, "Real-time motion planning with applications to autonomous urban driving," *IEEE Trans. Control Syst. Technol.*, vol. 17, no. 5, pp. 1105–1118, Jul. 2009, doi: 10.1109/TCST.2008.2012116.
[9] E. Frazzoli, "Quasi-random algorithms for real-time spacecraft motion planning and formation flight," *Acta Astronautica*, vol. 53, nos. 4–10, 2003, pp. 485–495, doi: 10.1016/S0094-5765(03)80009-7.
[10] E. Feron, M. Dahleh, E. Frazzoli, and R. Kornfeld, "A randomized attitude slew planning algorithm for autonomous spacecraft," in *Proc. AIAA Guid., Navigat., Control Conf. Exhibit*, Montreal, QC, Canada, Aug. 2012, p. 4155, doi: 10.2514/6.2001-4155.
[11] J. Phillips, L. Kavraki, and N. Bedrossian, "Spacecraft rendezvous and docking with real-time, randomized optimization," in *Proc. AIAA Guid., Navigat., Control Conf. Exhibit*, Austin, TX, USA, Jun. 2012, p. 5511, doi: 10.2514/6.2003-5511.
[12] M. Kobilarov and S. Pellegrino, "Trajectory planning for CubeSat short-time-scale proximity operations," *J. Guid., Control, Dyn.*, vol. 37, no. 2, pp. 566–579, Mar. 2014, doi: 10.2514/1.60289.
[13] J. A. Starek and B. W. Barbee, "A sampling based approach to spacecraft autonomous maneuvering with safety specifications," in *Proc. AAS GNC Conf.*, 2015, pp. 1–67.
[14] J. A. Starek, E. Schmerling, G. D. Maher, B. W. Barbee, and M. Pavone, "Real-time, propellant-optimized spacecraft motion planning under Clohessy-Wiltshire-Hill dynamics," in *Proc. IEEE Aerosp. Conf.*, Mar. 2016, pp. 1–16, doi: 10.1109/AERO.2016.7500704.
[15] J. A. Starek and E. G. D. Schmerling Maher, "Fast, safe, and propellant-efficient spacecraft planning under Clohessy-Wiltshire-Hill dynamics," *J. Guid., Control, Dyn.*, vol. 40, no. 2, pp. 418–438, 2017, doi: 10.2514/1.G001913.
[16] J. A. Starek, "Sampling-based path planning for safe and efficient spacecraft proximity operations," Ph.D. dissertation, Dept. Aeronaut. Astronaut., MIT, Cambridge, MA, USA, 2016.
[17] W. Fehse, *Automated Rendezvous and Docking of Spacecraft* (Cambridge Aerospace Series). Cambridge, U.K.: Cambridge Univ. Press, 2003, doi: 10.1017/CBO9780511543388.
[18] B. Naasz, "Safety ellipse motion with coarse sun angle optimization," in *Proc. SFC Flight Mech. Symp.*, Greenbelt, MD, USA, Oct. 2005, pp. 1–13.
[19] D. E. Gaylor and B. W. Barbee, "Algorithms for safe spacecraft proximity operations," *AAS/AIAA Spaceflight Mech. Meeting*, Sedona, Arizona, Jan. 2007, pp. 1–20.
[20] S. Di Cairano, H. Park, and I. Kolmanovsky, "Model predictive control approach for guidance of spacecraft rendezvous and proximity maneuvering," *Int. J. Robust Nonlinear Control*, vol. 22, no. 12, pp. 1398–1427, May 2012.

NING CHEN was born in 1990. She received the B.S. degree from Hebei University, China, and the M.E. degree from the University of South China. She is currently pursuing the Ph.D. degree with Space Engineering University. Her areas of research interest include space mission analysis and design, spacecraft dynamics, navigation and control, spacecraft proximity operation, and on-orbit service.

YASHENG ZHANG was born in 1974. She received the B.E. and M.E. degrees in spacecraft design and engineering from the National University of Defense Technology, China, and the Ph.D. degree from Space Engineering University. She is currently a Professor with Space Engineering University. Her areas of research interest include space mission analysis and design, spacecraft dynamics, and navigation and control.

ZHI LI was born in 1973. He received the B.E. and M.E. degrees in AI from the National University of Defense Technology, China, and the Ph.D. degree from Space Engineering University. He is currently a Professor with Space Engineering University. His areas of research interest include space mission analysis and design, spacecraft dynamics, navigation and control, and space security and strategy.

WENHUA CHENG was born in 1990. He received the B.E. degree in spacecraft design and engineering from the Harbin Institute of Technology, China, and the M.E. and Ph.D. degrees from Space Engineering University. He is currently a Lecturer with Space Engineering University. His areas of research interest include space mission analysis and design, spacecraft dynamics, navigation and control, and spacecraft proximity operation.

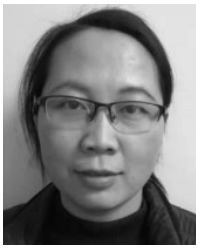

JILIAN LI received the B.E. and M.E. degrees in spacecraft design and engineering from the National University of Defense Technology, China, and the Ph.D. degree from Space Engineering University. She is currently an Associate Professor with Space Engineering University. Her areas of research interest include space mission analysis and design and space mission planning.

HUAFEI DIAO received the B.E., M.E., and Ph.D. degrees from Space Engineering University. He is currently an Associate Professor with Space Engineering University. His areas of research interest include space situational awareness, space mission analysis and design, and spacecraft orbital dynamics.

WEILIN WANG received the B.E., M.E., and Ph.D. degrees from the National University of Defense Technology, China. He is currently a Lecturer with Space Engineering University. His areas of research interest include on-orbit service, spacecraft dynamics, and navigation and control.

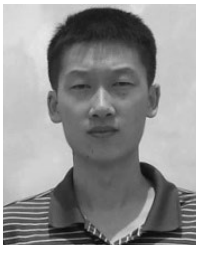

YUQIANG FANG received the B.E., M.E., and Ph.D. degrees from the National University of Defense Technology, China. He is currently a Lecturer with Space Engineering University. His areas of research interest include space situational awareness, AI in space, and spacecraft application.